Long plasma channels and high-voltage discharges induced by strong picosecond laser pulses

Hua Yang (杨 华)*, Xiaosong Tang (唐小松), Xingwei Zhang (张兴卫), Li Zhang (张 黎), Fuli Tan (谭福利), Jianheng Zhao (赵剑衡), and Chengwei Sun (孙承纬)**

Institute of Fluid Physics, China Academy of Engineering Physics, Mianyang 621900, China
**Corresponding author: yangqst@yahoo.com; **corresponding author: sunchengwei@hotmail.com*
Received August 15, 2015; accepted September 29, 2015; posted online October 21, 2015

The formation of long plasma channels and laser-induced high-voltage discharges are demonstrated by focusing infrared picosecond laser pulses in air. Based on measurements of the channel conductivity, the maximum electron density in excess of 10^{14} cm^{-3} is estimated. The plasma channels are good conductors, through which long-air-gap high-voltage discharges are triggered. The breakdown voltages show large drops but the discharging paths are not well guided: in this, the plasma spots distributed along the channel might play an important role.

OCIS codes: 320.5390, 350.5400, 140.3440.
doi: 10.3788/COL201513.113201.

Intense laser pulses launched in air can form thin columns of weakly ionized plasma, which can persist over long distances if the laser intensities are properly maintained. Laser-induced plasma channels hold great promise for a number of advanced technologies, including remote sensing[1–3], microwave channeling[4], and the remote manipulation of high-voltage (HV) discharges[5–9].

To date, extensive studies on laser-induced plasma channels have been carried out using infrared femtosecond lasers[10]. The low-energy femtosecond pulse focused in air can collapse into a thin filament with the diameter of about 100 μm and an electron density of about $10^{15} - 10^{16}$ cm^{-3}. In general, the propagation of the filament is maintained by a dynamic balance between self-focusing due to the optical Kerr effect and beam defocusing from free electrons[11], which is often not robust enough for long-range applications. Increasing the laser energy will eventually lead to multiple filaments[12], which can benefit the robust propagation over long distances but may introduce large complexity and instability due to multi-filament competition. Moreover, due to complex nonlinear effects, some important properties of the filaments, such as electron density, cannot be easily manipulated.

Strong picosecond laser pulses can offer another approach to produce and apply the laser-induced plasma channels. Provided with a relatively high power and high energy, effective ionization in air can also be achieved; thus, plasma channels can be effectively produced and maintained over relatively long ranges. The formation and application of long plasma channels using strong infrared picosecond laser pulses has great potential that is worth studying.

In this Letter, we present an experimental study on long-range plasma channels and HV discharges induced by strong infrared picosecond pulses focused in air. Long-range plasma channels with low resistances were effectively produced, along which plasma spots appeared and traced out along the channel path. The electron density depended on the laser energy, which might offer a new knob in various applications. Through the plasma channels, which are good conductors, laser-induced long-air-gap discharges under HV direct-current (DC) fields were triggered. The breakdown voltages showed large drops but the discharge paths were not well guided: in this, the plasma spots might play an important role.

The laser pulses were output from a picosecond Nd:YAG/YVO amplifier system with a maximum pulse energy of 100 mJ at 1064 nm, 10 Hz, and a pulse duration of 30 ps. The output beam diameter was 11 mm and the beam divergence was less than 0.5 mrad. To loosely focus the laser beam, a telescope-type double-lens system was employed. The effective focal distance could be controlled by changing the distance between the two lenses[13]. The focal lengths of the double lenses were 150 and −125 mm. In our experiment, the effective focal distance was kept at about 250 cm, where long plasma channels formed around the focus.

The channel paths became discernible in our dark laboratory due to small plasma spots, which distributed randomly along the channels. These plasma spots might derive from localized avalanche ionization[14]. Further growth of the plasma spots might be limit by the short pulse duration time; thus, the number and size of these spots remained small in each laser shot, and the laser propagation was not severely disturbed. As the laser was operated at a low repetition rate of 10 Hz, a color camera was employed to record the plasma spots over long exposures. These plasma spots can intuitively indicate the length and the intensity distribution of the plasma channel, as illustrated in Fig. 1(a). The channel paths persisting over long distances of more than 60 cm were clearly revealed by 30 s exposures. The lengths of the plasma channels could be controlled by the pulse energy. Different laser energies also led to different plasma

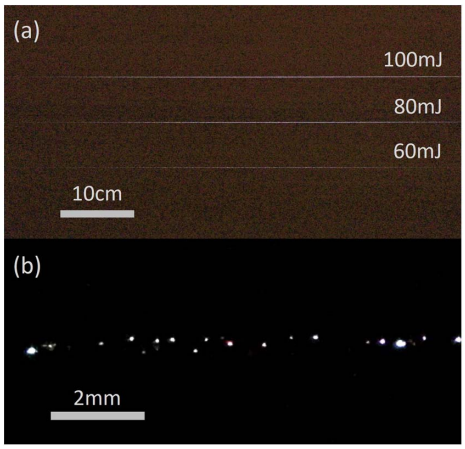

Fig. 1. (a) Plasma channel paths revealed by the plasma spots. (b) A detailed view of the plasma spots distribution after long exposures. The laser pulses propagate from right to left.

densities, which were reflected by the number of the plasma spots.

To give a detailed view of the plasma spots, we took a close-up photograph of the plasma channel near the focus of the double-lens system, as shown in Fig. 1(b). The laser energy was 100 mJ, while the exposure time was reduced to 8 s. The plasma spots were still visible at a shorter exposure, although the amount of the spots will correspondingly decrease. The plasma spots were spatially limited in a thin column about 450 μm in diameter and exhibited a random-like transversal distribution. The focal diameter of the double-lens system in the diffraction limit can be estimated by $d = 2.44f\lambda/D$, where f is the focal distance of the double-lens system and λ presents the laser wavelength. D is the diameter of the laser beam before the double lenses, which is about 12 mm, considering the beam divergence. The calculated focal diameter in the diffraction limit is about 540 μm, which is still larger than the channel diameter; thus, nonlinear effects such as the optical Kerr effect may play also a role in the maintenance of the long channel. The spot sizes varied between about 50 and 200 μm, with a typical size of about 100 μm. The sizes were comparable with the channel diameter, which indicated that the electron densities of these plasma spots were not high enough to severely disturb the laser propagation.

The ionization of air in the presence of a strong picosecond pulse takes place mainly by multi-photon ionization and avalanche ionization. The molecules are first ionized by multi-photon ionization, which offers electrons with a relatively low density. These electrons are then accelerated by the laser field and may collide with the molecules in air, which may free more electrons, resulting in an electron density that will grow in an avalanche-like manner. In the laser propagation, as the laser intensity distribution is not a perfect Gaussian shape, there may be some localized regions with higher laser intensities after focus, which may make the avalanche ionization happen more rapidly than in other places, resulting in plasma spots with higher electron densities. The presence of dust in the air may also lead to stronger ionization, but is not likely to be an important reason for the formation of these plasma spots in our experiment. As can be seen in Fig. 2(b), for each laser shot of maximum pulse energy, the average number of the plasma spots per centimeter was about 0.25, corresponding to a number density of about 1.6×10^8 m^{-3}, which is much larger than the number density of the dust (below 10^7 m^{-3} for dust particles with the diameters larger than 0.5 μm).

The channel conductivity was diagnosed using an electrical approach, through which we can estimate the electron density of the channel. A 40 nF capacitor serving as the high DC voltage supply and a sensing resistance of 50 Ω were connected with part of the plasma channel between two electrodes, which formed a simple circuit, as shown schematically in Fig. 2. The output voltage jitters were less than 1 kV during our experiment. The first electrode was a thin aluminum wire with the diameter of about 200 μm, which was carefully placed to contact the edge of the plasma channel. The second electrode was a 50 mm × 8 mm × 2 mm aluminum wire bundle that was simply inserted to cut off the laser path. After turning on the voltage supply, a transient circuit was formed by each laser shot. The current waveforms were obtained from a digital oscilloscope connected in parallel with the sensing resistance.

Typical current waveforms in the plasma channels under different laser energies are shown at the bottom of Fig. 2. The output voltage of 40 kV was adopted to overcome the environmental disturbance. The length of the central part of the channel chosen by the electrodes was 27 cm, in which the maximum current reached up to 110 mA at a pulse energy of 100 mJ. The corresponding resistance of 0.36 MΩ was comparable with or even lower

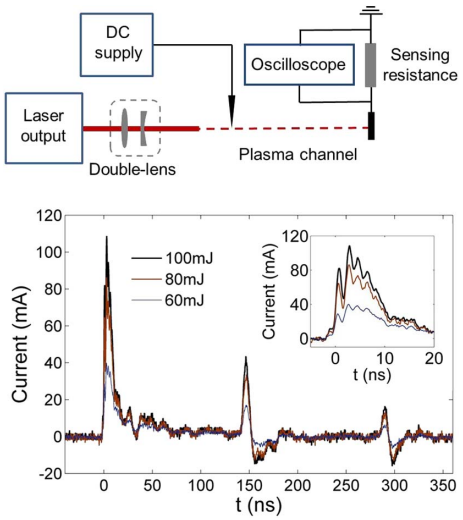

Fig. 2. Schematic of the conductivity measurements and the measured current waveforms at different laser energies. The inset shows the currents within 20 ns.

than the case of the femtosecond filaments[15]. The conductivity of the plasma column can be written as $\sigma = LR^{-1}A^{-1}$, where L is the channel length, R is the resistance, and A presents the cross-sectional area of the plasma column. The diameter of the plasma channel was estimated to be 450 μm, according to Fig. 2. We confirmed this value by measuring the diameter of the single-shot burning marks of the laser channel on glass and plastic surfaces, which gave similar results. The calculated conductivity according to the value of the maximum current at 100 mJ pulse energy is about 4.7 Ω^{-1} m^{-1}. The plasma density can be estimated from the conductivity through the expression $n_e = \sigma e^{-1}\mu_e^{-1}$, where e is the charge of an electron and μ_e presents the electron mobility. Assuming a low electron temperature, the adopted value of μ_e is 1600 cm^2 V^{-1} s^{-1}[15], and the maximum plasma density is calculated to be 1.8×10^{14} cm^{-3}. Note that the maximum of the current waveform appears at about 3 ns. The reason for the high-frequency oscillations in the first few nanoseconds is not confirmed, but according to the measured waveform, the initial electron density may have a similar value to the maximum electron density. The calculated density is relatively low compared with the typical maximum plasma density of about 10^{15} – 10^{16} cm^{-3} in femtosecond filaments[10]; however, the total resistance still remains small, which can be attributed to the large diameter. In air, electrons can attach to neutral oxygen molecules. This process, which occurs on a picosecond time scale, will make the electron density still underestimated using the electron mobility in our calculations. In fact, the mobility of positive and negative molecular oxygen ions may be a more relevant parameter[16]. We might also base the estimation on the multi-photon and avalanche ionization rates for air[17]. However, for pulses with a short duration time and high intensities above 10^{12} Wcm^{-2}, in these two ionization mechanisms, the estimated electron density is very sensitive to the laser intensity. Accurate values of the laser intensity as well as the electron removal processes may be important to make the estimation reliable. Note that the plasma spots were not considered in the estimation. For each laser shot, the amount of plasma spots was small. Although the plasma spots might have higher electron densities, they occupied a very small space; thus, they might have little influence in the measurements of the resistance. In particular, the plasma density depended on the laser energy, which may benefit various potential applications.

The lifetime of the plasma channels was shown to be about 8 ns in the full width at half-maximum (FWHM), according to the current waveforms. However, long tails of more than 100 ns were also observed. The currents revived at a time interval of about 150 ns, which was quite similar to the oscillation interpreted as the result of the virtual antenna effect in long plasma channels[18,19]. The low-frequency oscillations of the waveforms might originate from the longitudinal oscillation of the charged ions, which were strongly enhanced by the presence of the longitudinal static electric field.

Through the plasma channels, long air-gap discharges induced by strong picosecond laser pulses were realized. The experimental setup was similar to that described in Fig. 2. As the discharge current could be very large, it might cause damage to the vulnerable electrical components, such as the communication modules of the laser, which was placed in the same room as the HV supply. To avoid damage to the equipments caused by severe discharges, we removed the oscilloscope and replaced the sensing resistance with a 3 kΩ sodium chloride solution resistance. The sodium chloride solution resistance could endure very high voltages and limit the discharge currents. As the thin-wire electrode might explode when heated by a large discharge current, it was replaced by a thicker steel rod of 1 mm in diameter. At a given distance between the electrodes, the breakdown voltages without the laser were confirmed by increasing the applied voltage at a step of 1 kV until the discharge happened. The lowest breakdown voltages under laser inducement were confirmed in a similar manner, where we alternately increased the applied voltage and delivered a few laser pulses until the discharge was induced. The measured voltage fluctuations were about 2 kV. The discharge paths were recorded by a high-speed cameral that could capture 800 frames per second.

Figure 3(a) gives the breakdown voltages at different gap lengths, with or without the laser-induced plasma channel. A voltage drop of 23 kV was achieved at a gap length of 18 cm, which obviously indicated the trigger ability of the picosecond laser. The path of a spontaneous discharge, as well as two independent discharges induced by pulses of 100 mJ in energy, are illustrated in Fig. 3(b). The synchronization of the laser pulses and the induced discharges are indicated by the white sparks of scattered laser on the electrode, which were captured in same frame as the discharges. The HV breakdown occurred in less than 1.25 ms after the laser pulse. Limited by the temporal resolution of the high-speed cameral, the exact time delay of the HV breakdown could not be determined. Laser pulses play an important role in the beginning of the discharge. The initial electrons released by the multi-photon

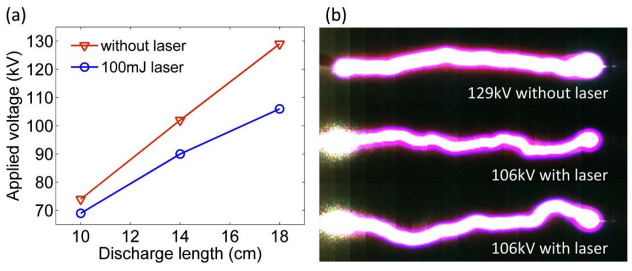

Fig. 3. (a) Breakdown voltages of spontaneous discharges and laser-induced discharges at different gap lengths. (b) Spontaneous discharge and induced discharges by pulses of 100 mJ in energy, where the laser pulses propagate from right to left and all the discharge lengths are 18 cm.

ionization of the laser field offer seeds for the following avalanche ionization. Heated by the HV field, a continuous discharge path can be finally developed[20].

It was suggested that the minimum initial electron density to trigger a discharge is less than 10^{12} cm^{-3}[21]. The electron density in our experiment far surpassed this critical value, which was the foundation of the effective laser-induced discharges. Moreover, the measured currents showed a long tail lasting more than 100 ns where the electron density is about $10^{12} - 10^{13}$ cm^{-3}. The elongation of plasma lifetime is still a major concern in research[22], as it will benefit very long-distance discharges. The intensity of the laser illuminated on the back electrode was high enough to create plasma plumes, which might also offer a certain amount of plasma close to the back electrode. But the gap lengths between the electrodes were generally in larger spatial scales than the plasma plumes. Thus, the effect of the laser illumination of the back electrode on the breakdown voltage decrease might be unimportant, although it could not be completely ignored.

As can be seen in Fig. 3(b), although the discharges were effectively triggered, the lightning paths were not well guided or even less smooth than the spontaneous discharge. It was suggested by Zhao *et al.*[21] that the triggered but not guided discharges occurr mostly in situations of localized ionization rather than a line of ionization. In our experiment, such localized ionization might exist in the form of the plasma spots shown in Fig. 2(b). For each laser shot of maximum pulse energy, the average number of plasma spots per centimeter was about 0.25; thus, on average, there were about 4–5 plasma spots in the 18 cm discharge path. In general, the plasma column was ohmically heated by the DC field. However, in the plasma spots, the optical heat of the laser, which could transfer energy from the electrons to the gas molecules, might also be important[23]. Although here it only happened in the early stage and was limited by the short pulse duration, these regions with a high initial electron density might be ohmically heated by the DC field more effectively. Each of them had a higher electron density than the other parts of the channel, and thus would probably grow much faster. The uniformity of the field was reduced, and the charge might migrate not only along the laser beam, but also transversely, toward the regions of high field gradient. As the plasma spots were randomly distributed, the lightning paths were also random.

Early experiments on long-distance discharge inducements using high-energy nanosecond lasers often suffered from the absorption of the laser energy by plasma sparks. One suggested solution was using multi-beam systems[24], where each beam produces a short conducting part. It was quite difficult to realize in practice. Here, it becomes much more practical, because we are using strong picosecond lasers. The plasma spots might act as the short conducting parts that were formed in a single laser beam, while the amount of these plasma spots depended on the pulse energy. Our results suggest an approach of a large potential in long-distance discharge inducement.

In conclusion, long-range plasma channels are produced by focusing strong infrared picosecond pulses in air. Plasma spots appear in the channels; these indicate the diameter, length, and plasma intensity distribution. The estimated maximum electron density reaches 10^{14} cm^{-3} in the plasma channels. Benefited by the large diameter size, the channels are good conductors. We achieve long air-gap laser-induced discharges through the conducting plasma channels, although the discharge paths are not well guided, which implies that the plasma spots might play an important role. As the laser energies in our experiment are limited, the plasma density is relatively low compared with the typical maximum plasma density of about $10^{15} - 10^{16}$ cm^{-3} in femtosecond filaments. Plasma channels with longer lengths and higher plasma densities can be achieved using more powerful picosecond lasers, where the high controllability, relatively low cost, and easy operation of picosecond laser systems may benefit various applications in the future.

References

1. J. Kasparian, M. Rodriguez, G. Méjean, J. Yu, E. Salmon, H. Wille, R. Bourayou, S. Frey, Y. B. André, A. Mysyrowicz, R. Sauerbrey, J. P. Wolf, and L. Wöste, Science **301**, 61 (2003).
2. A. Dogariu, J. B. Michael, M. O. Scully, and R. B. Miles, Science **331**, 442 (2011).
3. T. Wang, S. Yuan, Y. Chen, and S. L. Chin, Chin. Opt. Lett. **11**, 011401 (2013).
4. M. Chateauneuf, J. Dubois, S. Payeur, and J. C. Kieffer, Appl. Phys. Lett. **92**, 091104 (2008).
5. R. Ackermann, G. Méchain, G. Méjean, R. Bourayou, M. Rodriguez, K. Stelmaszczyk, J. Kasparian, J. Yu, E. Salmon, S. Tzortzakis, Y. B. André, J. F. Bourrillon, L. Tamin, J. P. Cascelli, C. Campo, C. Davoise, A. Mysyrowicz, R. Sauerbrey, L. Wöste, and J. P. Wolf, Appl. Phys. B **82**, 561 (2006).
6. Y. Brelet, A. Houard, L. Arantchouk, B. Forestier, Y. Liu, B. Prade, J. Carbonnel, Y. B. André, and A. Mysyrowicz, Appl. Phys. Lett. **100**, 181112 (2012).
7. M. Rodriguez, R. Sauerbrey, H. Wille, L. Wöste, T. Fujii, Y. B. André, A. Mysyrowicz, L. Klingbeil, K. Rethmeier, W. Kalkner, J. Kasparian, E. Salmon, J. Yu, and J. P. Wolf, Opt. Lett. **27**, 772 (2002).
8. S. B. Leonov, A. A. Firsov, M. A. Shurupov, J. B. Michael, M. N. Shneider, R. B. Miles, and N. A. Popov, Phys. Plasmas **19**, 123502 (2012).
9. M. Clerici, Y. Hu, P. Lassonde, C. Milián, A. Couairon, D. N. Christodoulides, Z. Chen, L. Razzari, F. Vidal, F. Légaré, D. Faccio, and R. Morandotti, Sci. Adv. **1**, e1400111 (2015).
10. A. Couairona and A. Mysyrowicz, Phys. Rep. **441**, 47 (2007).
11. R. Xu, Y. Bai, L. Song, N. Li, P. Peng, and L. Peng, Chin. Opt. Lett. **11**, 123002 (2013).
12. Z. Q. Hao, J. Zhang, T. T. Xi, X. H. Yuan, Z. Y. Zheng, X. Lu, M. Y. Yu, Y. T. Li, Z. H. Wang, W. Zhao, and Z. Y. Wei, Opt. Express **15**, 16102 (2007).
13. S. Eisenmann, E. Louzon, Y. Katzir, T. Palchan, A. Zigler, Y. Sivan, and G. Fibich, Opt. Express **15**, 2779 (2007).
14. C. G. Durfee, J. Lynch, and H. M. Milchberg, Phys. Rev. E **51**, 2368 (1995).
15. R. P. Fischer, A. C. Ting, D. F. Gordon, R. F. Fernsler, G. P. DiComo, and P. Sprangle, IEEE Trans. Plasma Sci. **35**, 1430 (2007).
16. P. Polynkin, Appl. Phys. Lett. **101**, 164102 (2012).

17. A. Sircar, R. K. Dwivedi, and R. K. Thareja, Appl. Phys. B **63**, 623 (1996).
18. G. Méchain, A. Mysyrowicz, M. Depiesse, and M. Pellet, Proc. SPIE **5989**, 59890S (2005).
19. B. Forestier, A. Houard, M. Durand, Y. B. André, B. Prade, J. Y. Dauvignac, F. Perret, Ch. Pichot, M. Pellet, and A. Mysyrowicz, Appl. Phys. Lett. **96**, 141111 (2010).
20. D. F. Gordon, A. Ting, R. F. Hubbard, E. Briscoe, C. Manka, S. P. Slinker, A. P. Baronavski, H. D. Ladouceur, P. W. Grounds, and P. G. Girardi, Phys. Plasmas **10**, 4530 (2003).
21. X. M. Zhao, J. C. Diels, C. Y. Wang, and J. M. Elizondo, IEEE J. Quantum Electron. **31**, 599 (1995).
22. X. L. Liu, X. Lu, J. L. Ma, L. B. Feng, X. L. Ge, Y. Zheng, Y. T. Li, L. M. Chen, Q. L. Dong, W. M. Wang, Z. H. Wang, H. Teng, Z. Y. Wei, and J. Zhang, Opt. Express **20**, 5968 (2012).
23. M. Scheller, N. Born, W. Cheng, and P. Polynkin, Optica **1**, 125 (2014).
24. T. Shindo, Y. Aihara, M. Miki, and T. Suzuki, IEEE Trans. Power Delivery **8**, 311 (1993).